Supplemental Figures

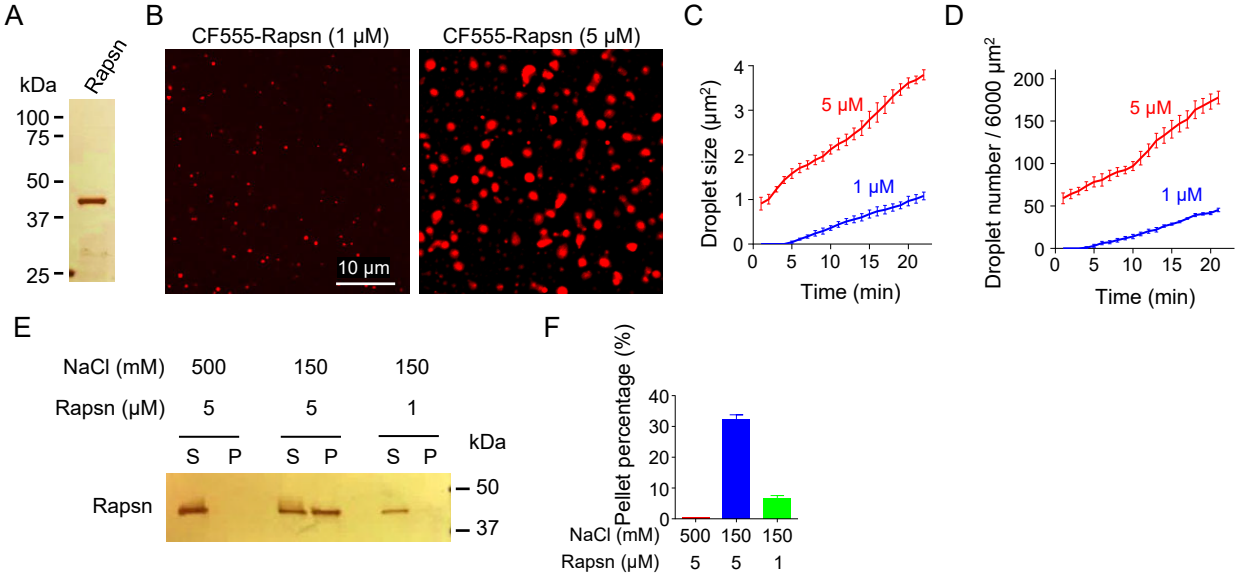

Figure S1. LLPS of Rapsn into condensates in vitro, Related to Figure 1.

(A) Silver staining showing purified Rapsn.
(B-D) Rapsn was able to phase separate into condensed droplets in a concentration-dependent manner.
(B) CF555-labeled Rapsn (1 μM and 5 μM) was able to phase separate into condensed droplets.
(C, D) Quantification of the droplet size and number formed by Rapsn (1 μM and 5 μM) at different time points. Data was shown as mean ± SEM; n = 3.
(E) Representative silver staining analysis showing the distribution of Rapsn in aqueous phase (S) and condensed phase (P) under different protein concentrations in the buffer containing 25 mM Tris, pH7.4, 5 mM DTT, and 150 mM NaCl or 500 mM NaCl.
(F) Quantification of percentage of Rapsn in pellets in (E). Data was shown as mean ± SEM; n = 3.

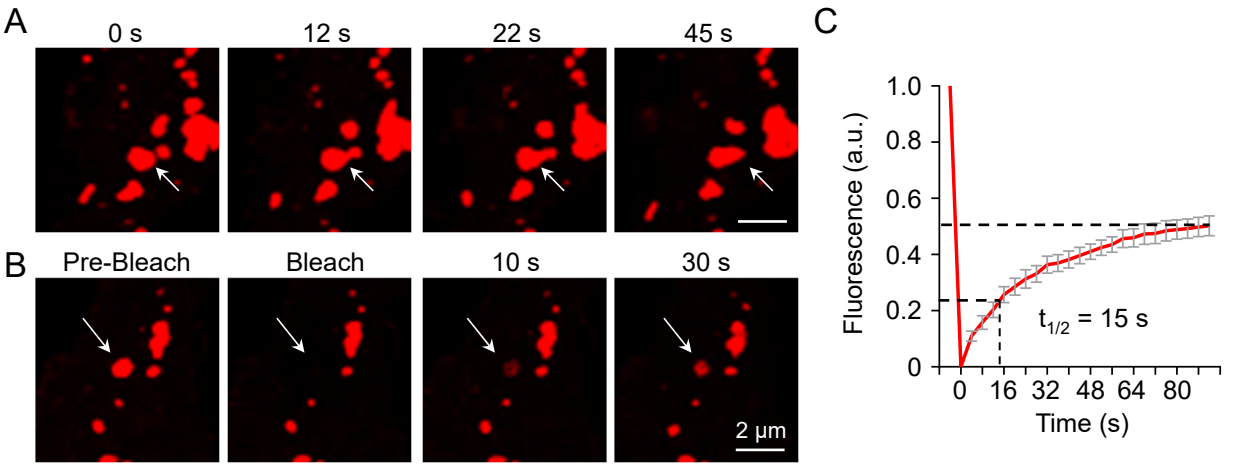

Figure S2. LLPS of Rapsn-mCherry into liquid-like compartments in HEK293T cells, Related to Figure 2.

(A) Fusion of two Rapsn-mCherry puncta in HEK293T cells.
(B) FRAP analysis showing dynamic exchange of Rapsn-mCherry between puncta and surrounding milieu.
(C) Quantification of fluorescence recovery in (B). Data were shown as mean ± SEM; n = 10.

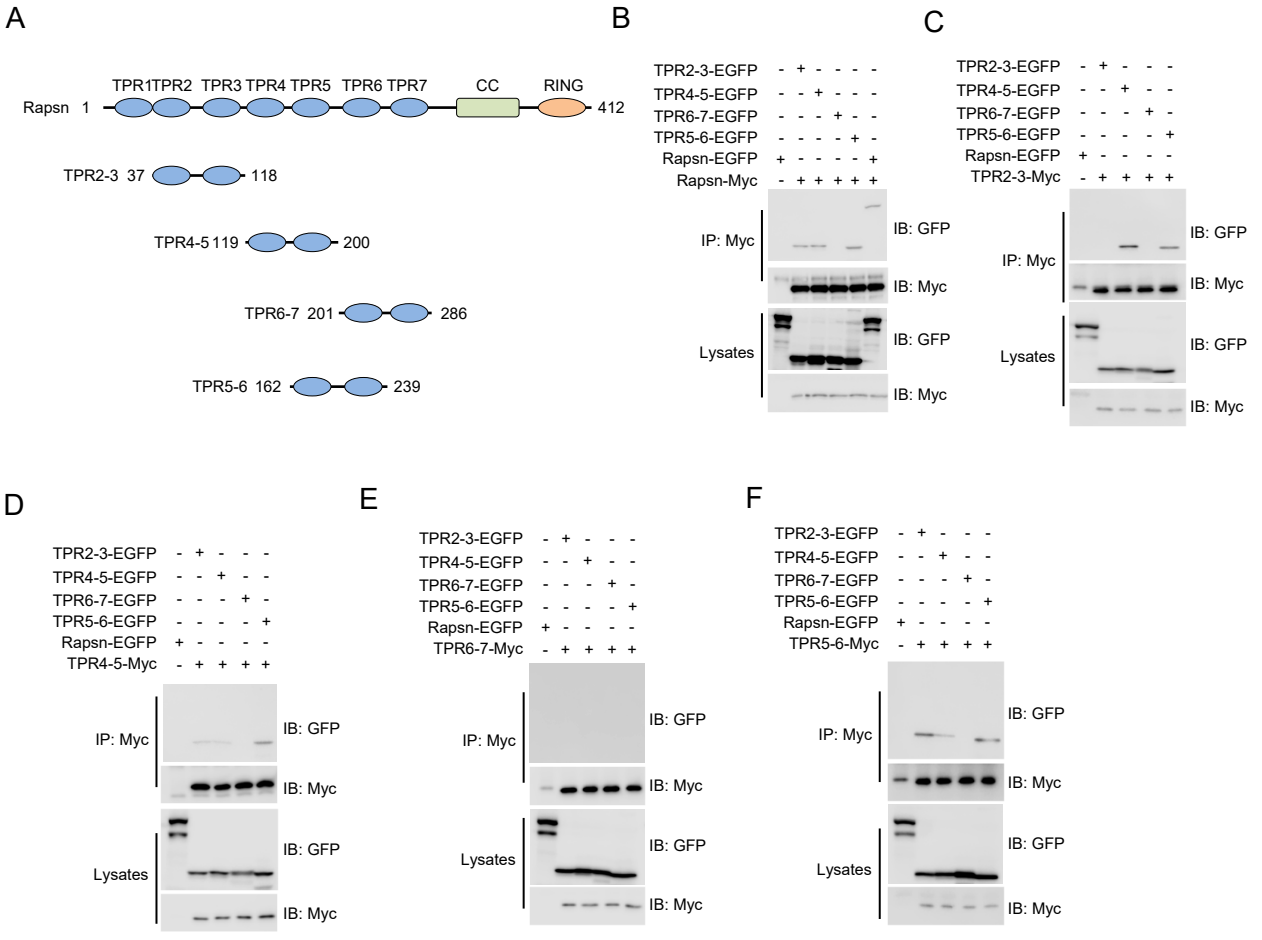

Figure S3. Multivalent binding of the TPR region, Related to Figure 4.

(A) Schematic diagram showing Rapsn domain structure, and various truncated proteins.
(B) Binding of Rapsn with TPR2-3, TPR4-5, TPR5-6, but not TPR6-7. EGFP-tagged TPR2-3, TPR4-5, TPR6-7, or TPR5-6 was cotransfected with Myc-tagged Rapsn into HEK293T cells. 48 hr later, cells were lysed and incubated with anti-Myc beads to precipitate Rapsn-Myc. Resulting complex was probed with indicated antibodies.
(C-F) TPR2-3, TPR4-5 or TPR5-6, but not TPR6-7 was able to bind with one another. The binding of TPR2-3-Myc (C), TPR4-5-Myc (D), TPR6-7-Myc (E), or TPR5-6-Myc (F) with EGFP-tagged TPR2-3, TPR4-5, TPR6-7, and TPR5-6 was characterized by co-immunoprecipitation.

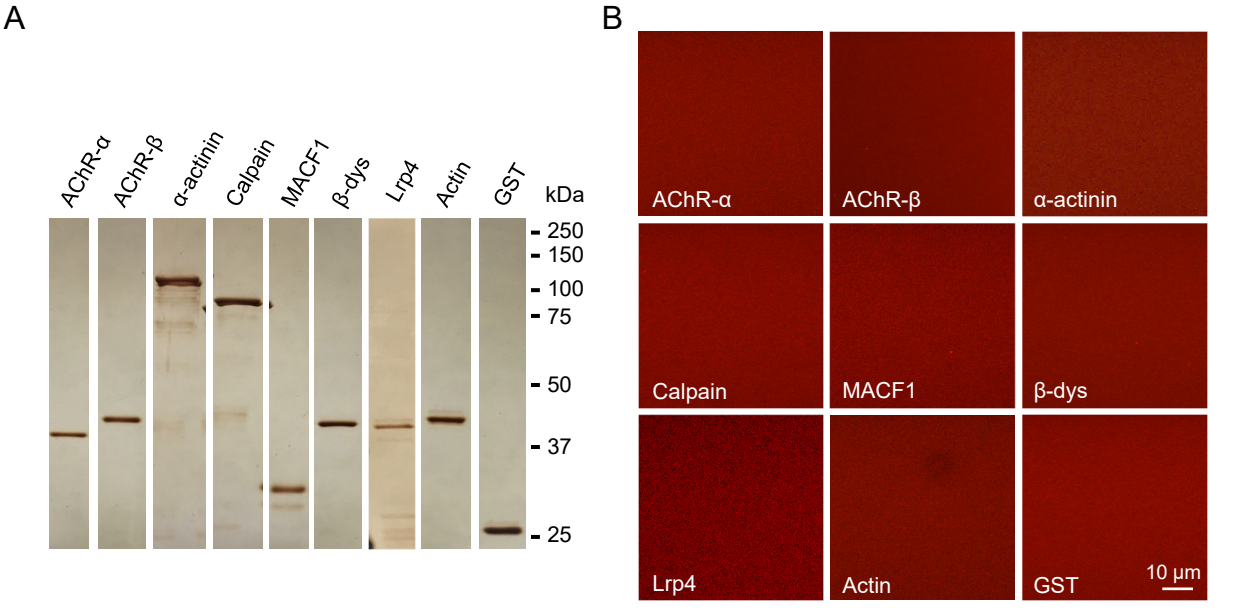

Figure S4. Failure of cargo proteins to phase separate into condensates by themselves, Related to Figure 5.

(A) Rapsn cargo proteins, as well as GST, Lrp4 and actin, were purified and examined by silver staining.
(B) Purified proteins were labeled with CF555, and their ability to form droplets was examined. Note that none of them was unable to phase separate into droplets.

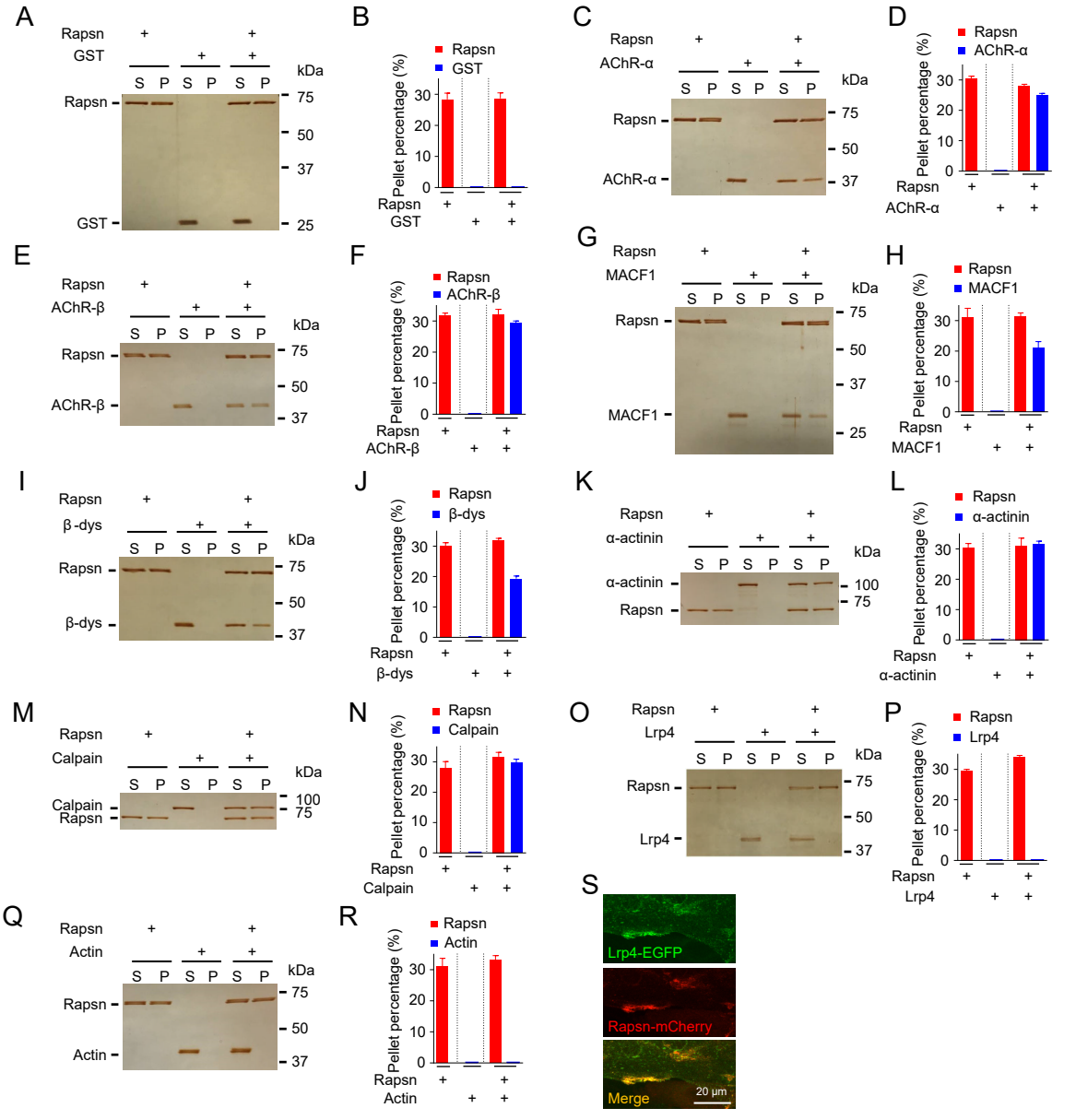

Figure S5. Recruitment of cargo proteins into Rapsn LLPS-mediated condensates, Related to Figure 5.

(A, B) GST was unable to be incorporated in Rapsn LLPS-mediated condensates.

(A) Representative silver staining image showing distribution of Rapsn-EGFP and GST in aqueous phase (S) and condensed phase (P) by Rapsn-EGFP (5 μM), GST (5 μM), or mixture containing Rapsn-EGFP (5 μM) and GST (5 μM). Note that GST was undetectable in pellets when examined alone or mixed with equimolar Rapsn-EGFP.

(B) Quantification of pellet percentage of Rapsn-EGFP and GST in different groups in (A). Data were shown as mean ± SEM; n = 3.

(C-R) AChR-α (C, D), AChR-β (E, F), MACF1 (G, H), β-dystroglycan (I, J), α-actinin (K, L) and calpain (M, N), were detectable in pellets when mixed with Rapsn-EGFP, but not alone. Lrp4 (O, P) or Actin (Q, R) was undetectable in pellets when examined alone or mixed with equimolar Rapsn-EGFP. Data were shown as mean ± SEM; n = 3.

(S) Colocalization of Lrp4-EGFP and Rapsn-mCherry in myotubes. Myoblasts were cotransfected with Lrp4-EGFP and Rapsn-mCherry. Resulting myotubes were treated with agrin for 12 hr and examined for co-distribution of Lrp4-EGFP and Rapsn-mCherry.

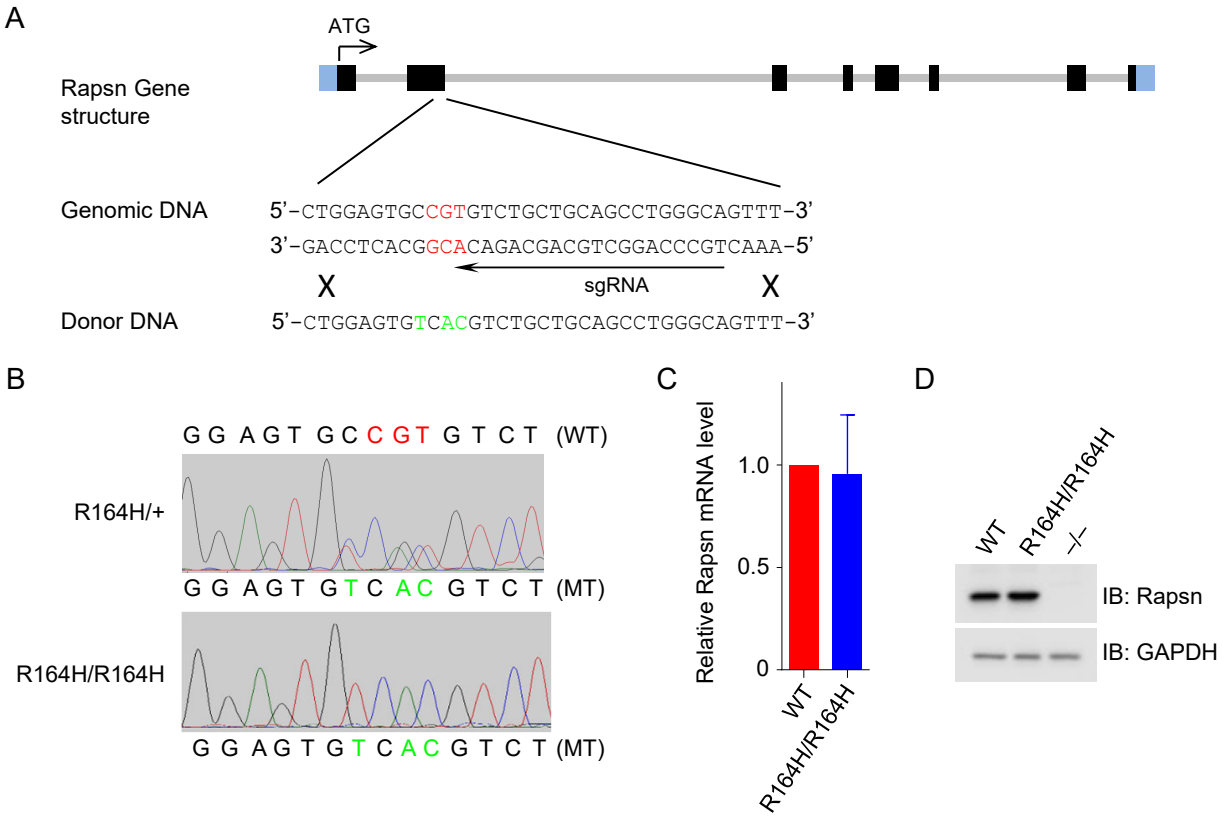

Figure S6. Generation of R164H knockin mutant mice by CRISPR-Cas9, Related to Figure 8.

(A) Generation of R164H knockin mutant mice by CRISPR-Cas9. Illustration of CRISPR-Cas9 strategy to generate R164H knockin mutant mice. The codon encoding R164 in genomic DNA was indicated in red. Mutated base pairs in donor DNA were indicated in green.

(B) Verification of R164H mutation by genomic DNA sequencing. Genomic DNA of indicated genotypes was sequenced. WT R164 was highlighted in red, and mutated base pairs were indicated in green.

(C) Comparable mRNA levels of Rapsn in WT and R164H/R164H mutant mice. Data were shown as mean ± SEM; n = 3, Student T-test.

(D) Similar Rapsn protein levels between WT and R164H/R164H mutant mice.

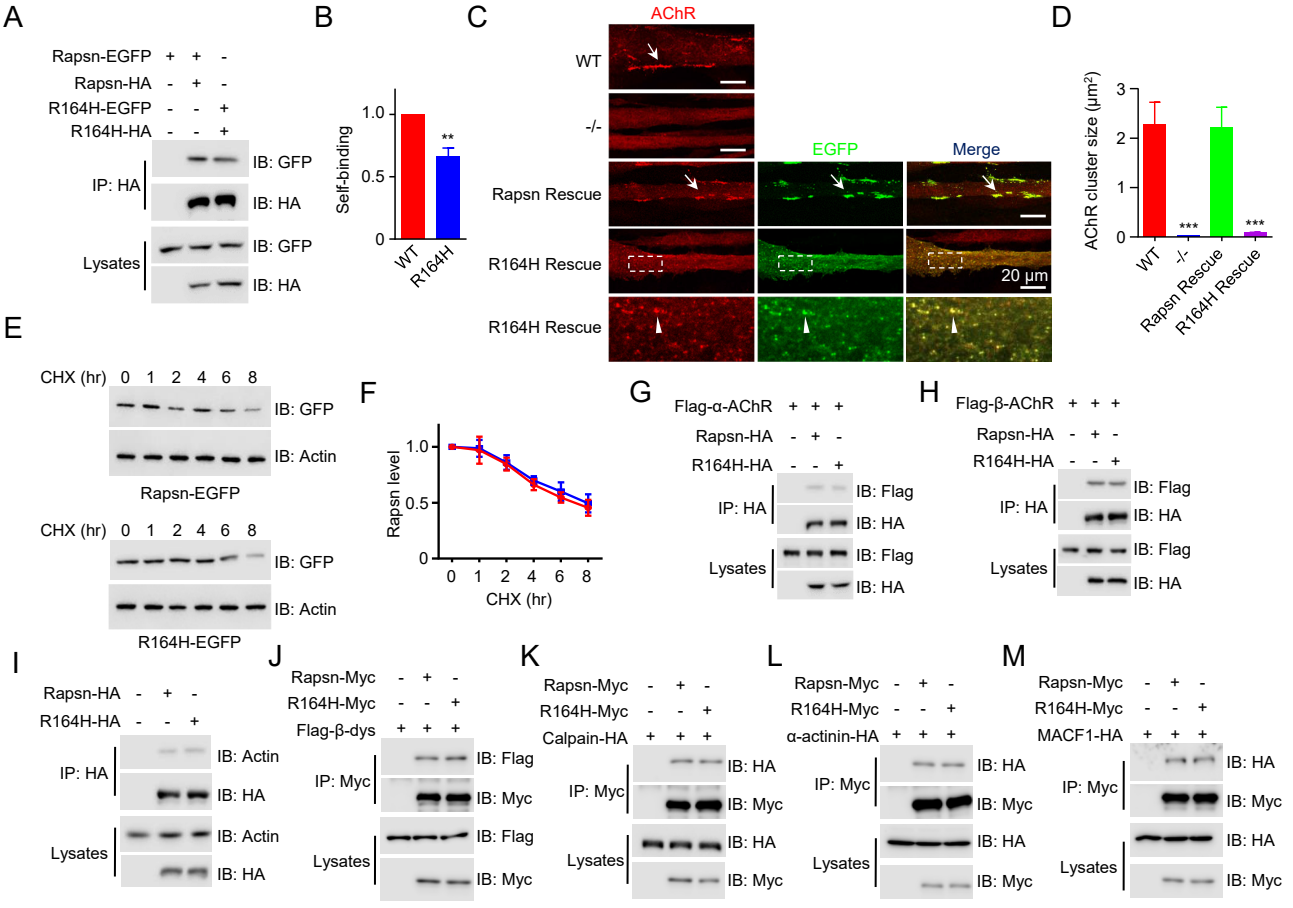

Figure S7. R164H is impaired in self-association and in rescuing AChR clustering in Rapsn -/- myotubes, Related to Figure 8.

(A, B) Reduced Rapsn self-association by R164H mutation. Data were shown as mean ± SEM; n = 3; **, P < 0.01; Student T-test.

(C, D) Failure of R164H mutant Rapsn in rescuing agrin-induced AChR clusters in Rapsn -/- myotubes.

(C) WT, Rapsn -/-, or Rapsn -/- myotubes transfected with EGFP-tagged WT or R164H mutant Rapsn was treated with agrin for 12 hr and stained with Flour 594-α-BTX (red) to label AChR clusters. Arrows, large AChR or Rapsn-EGFP clusters; arrow heads, small AChR or R164H-EGFP clusters.

(D) Quantification of AChR cluster size in (C). Clusters (> 0.01 μm2) identifiable by ImageJ were quantified. Data were shown as mean ± SEM; n = 3; ***, P < 0.001; One-way ANOVA.

(E, F) Comparable degradation of WT and R164H mutant Rapsn in HEK293T cells. HEK293T cells were transfected with EGFP-tagged WT or R164H mutant Rapsn. After 12 hr, cells were separated into 6-well plates and cultured for additional 12 hr. Cells were treated with CHX (50 μM) for indicated times; resulting lysates were blotted with anti-GFP antibody. (F) Quantitative data in (E). Data were shown as mean ± SEM; n = 3; Student T-test.

(G, H) Comparable interaction of WT and R164H mutant Rapsn with AChR subunits examined by co-immunoprecipitation assay.

(I) Comparable binding of WT or R164H mutant Rapsn with actin. HA-tagged WT or R164H mutant Rapsn was transfected into myoblasts. Resulting myotubes were lysed and the interaction of Rapsn and actin was examined by co-immunoprecipitation assay.

(J-M) Comparable binding of WT and R164H Rapsn with β-dystroglycan (J), calpain (K), α-actinin (L), or MACF1 (M) examined by co-immunoprecipitation.

Supplmental Table

Table S1. Effects of CMS mutations on Rapsn LLPS and co-condensation with cargo proteins, Related to Figure 7.

CMS mutations	LLPS	Co-condensation					
		AChR-α	AChR-β	MACF1	β-dys	α-actinin	Calpain
Q3K	-	-	-	-	-	-	-
L14P	↓	NA	NA	NA	NA	NA	NA
A73D	-	-	-	-	-	-	-
N88K	↓	NA	NA	NA	NA	NA	NA
R91L	-	-	-	-	-	-	-
A142D	-	-	-	-	-	-	-
E147K	-	-	-	↓	-	-	-
R164H	↓	NA	NA	NA	NA	NA	NA
L169P	-	-	-	-	-	-	-
R242W	-	-	-	-	-	-	-
L283P	-	-	-	-	-	-	-
L326P	-	↓	↓	-	-	-	-
C366A	-	-	-	-	-	-	-
1177del2	-	-	-	-	↓	-	-

"↓", reduced; "-", no effect; "NA", not applicable